Brazilian Journal of Geophysics, **42** (2024), 2, 1–25
Brazilian Geophysical Society
ISSN 2764-8044
DOI 10.22564/brjg.v42i2.2312

PETROPHYSICAL PARAMETERS AND ELECTROFACIES MODELS OF THE ITARARÉ GROUP APPLYING MULTI-RESOLUTION GRAPH-BASED CLUSTERING METHOD, PARANÁ BASIN

Marco Antônio R. de Almeida *, Marivaldo dos Santos Nascimento and Marvim Francis Mota Alves

Universidade Federal de Santa Catarina - UFSC, PPGGeologia, DGL, Florianópolis, SC, Brazil

*Corresponding author: mar.almeida@outlook.com

ABSTRACT. The volume shale (V_{sh}) and the effective porosity (ϕe) were calculated and partially applied as petrophysical input parameters to generate electrofacies models using the Multi-Resolution Graph-Based Clustering method in sedimentary successions of the Itararé Group. The petrophysical parameters and electrofacies models were determined from geophysical data from two wells located in the eastern portion of the Paraná Basin. The stratigraphic intervals in each well (analogues of hydrocarbon reservoirs) allowed the petrophysical analysis and the determination of electrofacies models based on gamma ray profiles, apparent density and neutron porosity, together with lithological data. The petrophysical parameters were calculated by different procedures, and the effective porosity results were applied as input parameters for electrofacies modeling. The electrofacies models were correlated to lithological data and patterns of gamma ray profiles and apparent density, as well as different types of porosity. The generated models provide differences related to the type of porosity, the method applied to calculate the effective porosity and present probable relationships with the lithological units of the wells.

Keywords: volume shale; porosity; bulk-density; gamma ray; stratigraphy

INTRODUCTION

Petrophysical analysis is one of the most useful and important tools available for reservoir characterization as it helps to define physical rock characteristics based on well log data. The petrophysical analysis includes the determination of parameters such as lithology, volume shale, porosity, water saturation, hydrocarbon saturation, pore geometry and permeability. Well log data are also used to identify productive zones, to determine depth and thickness of zones, to distinguish oil, gas and water zones in a reservoir, and to estimate hydrocarbon reserves. Furthermore, geologic maps developed from log interpretation are useful in determining facies relationships and drilling locations Asquith et al. (2004).

Electrofacies are unique combinations of petrophysical log responses that reflect specific physical and compositional characteristics of a rock interval cut by a borehole (Serra and Abbott, 1982; Sagar et al., 2018). Electrofacies characterization is widely used in petroleum prospecting, and it is an essential component for reservoir characterization. It involves partitioning a set of log data into electrofacies units and presenting them in a manner that is comparable to that used by geologists for either outcrop or core description (Ye and Rabiller, 2005).

In the Paraná Basin (see Figure 1a), the Itararé Group includes Permo-Carboniferous stratigraphic intervals of sandstone, which are considered analogues of hydrocarbon reservoirs (França and Potter, 1988; Bocardi et al., 2006; Buso et al., 2019). The geophysical and geological data conceded by the Agência Nacional do Petróleo, Gás Natural e Biocombustíveis (ANP) of wells 1GO-1-SC and 1RCH-1-SC in western Santa Catarina state (see Figure 1b) were used

to determine petrophysical parameters, such as volume shale (V_{sh}) and effective porosity (ϕ_e) for the intervals corresponding to the Itararé Group. These parameters were obtained using different methods, so that the effective porosity results were then evaluated for each well and used as one of the input parameters to generate electrofacies models applying the Multi-Resolution Graph-Based Clustering (MRGC) method (Ye and Rabiller, 2000). The MRGC method is a multi-dimensional dot-pattern recognition method that distinguishes natural data groups, based on non-parametric k-nearest neighbors and graph data representation, not requiring priori knowledge of the data set (Ye and Rabiller, 2000). This method was applied in order to combine the effective porosity results (ϕ_e), neutron porosity (NPHI), gamma ray (GR) and bulk-density (RHOB), in distinct arrangements within the lithological data, resulting into four electrofacies models. This paper aims to determine the petrophysical parameters of Vsh and (ϕ_e) for the intervals corresponding to the Itararé Group in the mentioned wells, and to propose electrofacies models based on different types of porosity, allowing methodological comparatives and analysis of possible relationships for the lithological intervals of the wells.

GEOLOGICAL CONTEXT

The Paraná Basin (Almeida et al., 1977) comprises a wide sedimentary area of approximately 1,500,000 km² whose geological history is related to cycles of tectonic subsidence and uplift that gave rise to six Supersequences limited at the top and base by unconformities (Milani et al., 2007, see Figure 1a): Rio Ivaí (Ordovincian-Silurian), Paraná (Devonian), Gondwana I (Carboniferous-Eotriassic), Gondwana II (Meso-Neo-Triassic), Gondwana III (Neo-Jurassic-Eocretaceous) and Bauru (Neo-Cretaceous).

The tectono-stratigraphic evolution of the Paraná Basin is related to the development of collisional Precambrian continental crust on the southwestern margin of the Gondwana Supercontinent, which consists of several cratonic nuclei bounded by orogenic belts composed of thrusted metasedimentary rocks intruded by granites (Eyles et al., 1993, see Figure 2a).

The Itararé Group is approximately 1300 m thick and comprises the Lagoa Azul, Campo Mourão and Taciba formations (França, 1987; França and Potter, 1991; Milani, 2004, see Figure 2b). As a result of the Serra Geral Group volcanic rock cover, only 5% by area of the Paraná Basin sedimentary fill is exposed (see Figure 1a). According to Eyles et al. (1993), the oldest Itararé sedimentary succession records a glacio-lacustrine setting though it is possible to identify an increasing marine influence upwards through the Itararé Group. The fully marine conditions are recorded by the overlaying deltaic successions on the top of this Group. Based on core examinations of 107 wells across the basin, Eyles et al. (1993) estimated a total logged section of over 1700 m within the Itararé Group, which comprises diamictite, conglomerate, sandstone, siltite and shale.

METHODS

The determination of petrophysical parameters and the electrofacies modeling for the Itararé Group intervals were conducted utilizing well data provided by ANP to the project titled *Técnicas Machine Learning para Reconhecimento de Padrões Sedimentológicos de Sistemas Turbidíticos - MLTurb*. The methodological approach encompasses four key steps:

i. The database structuring consisted of the integration of DLIS well files into the *Geolog software*, followed by data evaluation and systematic arrangement, in layouts, of the geophysical logs in conjunction with lithological data for each well. The logs utilized in this step were: GR, RHOB and NPHI, standardized in API units, kg/m^3 and V/V, respectively. The lithological data, available in AGP files (General Data Archive), were tabulated in CSV format to allow the generation of lithology intervals for each well into the *Geolog software*. The layouts, which reunite the GR, RHOB and NPHI logs in conjunction with the lithological intervals, were generated to assist the determination of petrophysical parameters and the electrofacies modeling steps.

ii. The Volume shale (V_{sh}) was determined using the gamma ray index (IGR) (Asquith and Gibson, 1982), expressed as:

$$IGR = \frac{(GR - GR_{min})}{(GR_{max} - GR_{min})}, \tag{1}$$

where GR is the gamma ray reading of the formation (in API); GR_{min} represents the minimum gamma ray reading in the formation (usually found in the cleanest sandstone or limestone layers); and GR_{max}, which represents the maximum gamma ray reading in the formation (typically found in the purest shale layers). The gamma ray index was also used to determine the Volume shale using the Larionov method (Larionov, 1969), expressed as:

$$V_{sh_{lar}} = 0.33(2^{2IGR} - 1), \tag{2}$$

The IGR and Larionov method results were compared for all lithological intervals, in order to evaluate the discrepancy (D) between these methods, expressed as:

$$D = |\overline{IGR} - \overline{V_{sh_{lar}}}|, \tag{3}$$

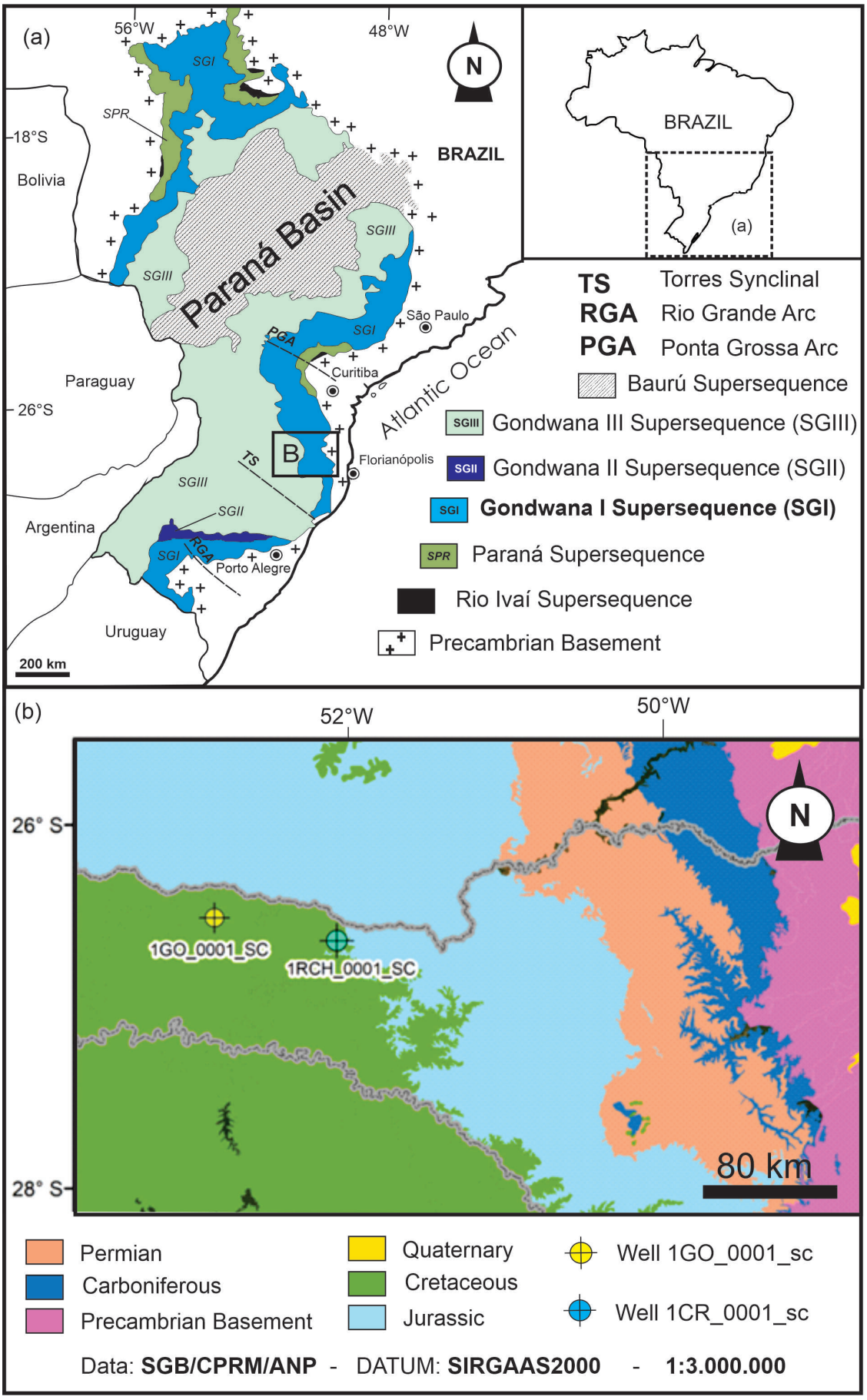

Figure 1: (a) Simplified geologic map of the Paraná Basin with the stratigraphic Supersequences (after Milani et al. (1994)); and (b) Geological map (from SGB) with locations of wells 1GO1SC and 1RCH1SC (from ANP) in western Santa Catarina state.

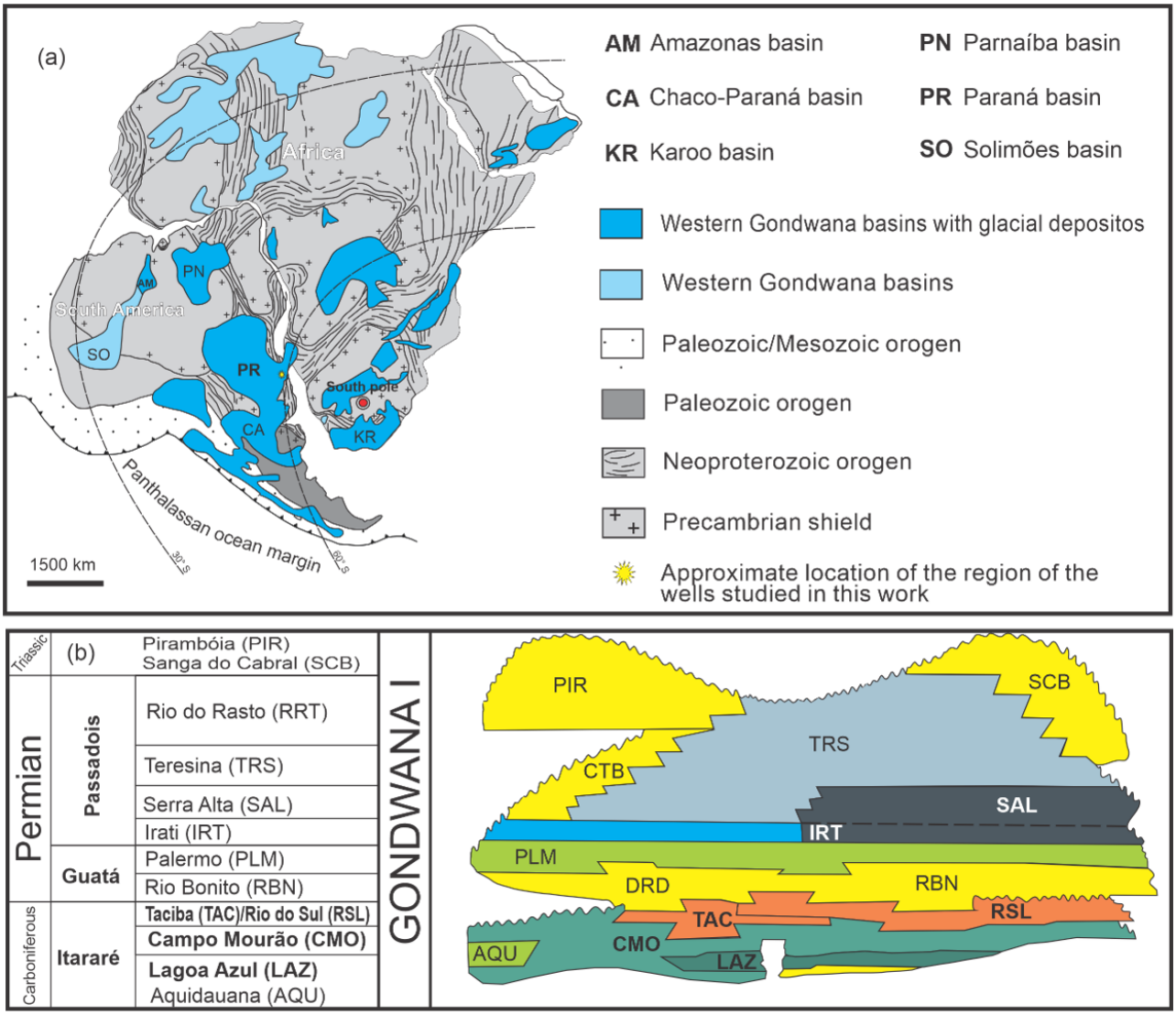

Figure 2: (a) Geological reconstruction of West Gondwana (adapted from Malone et al., 2008; Meert et al., 2010) and (b) Stratigraphic chart of the Gondwana I Supersequence (from Milani, 2004).

where $\overline{IGR}$ is the mean V_{sh} value for a given lithological interval, obtained by the gamma ray index, while $\overline{V_{sh_{lar}}}$ is the mean V_{sh} value for a given lithological interval, obtained by the Larionov method.

iii. The effective porosity (ϕe) was determined using the density method (ϕe_D) (Asquith and Gibson, 1982) and the neutron-density method (ϕe_{ND}) (Bateman and Konen, 1977). The effective porosity from the density method is basically obtained from the density-porosity formula, adjusted to the effect caused by the presence of shales in the total porosity of a formation, as expressed in the following equation:

$$\phi e_D = \frac{\rho_m - \rho_b}{\rho_m - \rho_f} - V_{sh}\frac{\rho_m - \rho_{sh}}{\rho_m - \rho_f}, \qquad (4)$$

where ρ_m is the rock matrix density, or the solid framework density of the formation (in kg/m^3); ρ_b represents the bulk-density readings from RHOB log (in kg/m^3); ρ_f corresponds to the density of the fluid existing in the formation (in kg/m^3); ρ_{sh} corresponds to the representative density value for shales (kg/m^3); and V_{sh} (V/V) represents the volume shale of the formation. The effective porosity using the neutron-density method (ϕe_{ND}) consists of a crossplot of the results obtained from Equation(4) with the results of the effective porosity obtained from the neutron porosity log (NPHI), the last being determined by the following expression:

$$\phi e_N = \phi_N - V_{sh}\phi_{Nsh}, \qquad (5)$$

where ϕ_N corresponds to the neutron porosity readings from the NPHI log (in V/V);ϕ_{NSh} is the representative neutron porosity value for shales (in V/V); and V_{sh} corresponds to the volume shale of the formation (in V/V). The neutron-density method ϕe_{ND} calculation is automatically executed by the Geolog Software (Emerson), as long the analyst provides all required input data. All logs and constants required to calculate ϕe (using both methods) were available in the well files. The V_{sh} results utilized for the calculation of both ϕe_D and ϕe_{ND} were those obtained from Equation(2), since the Itararé Group comprises rocks older than Tertiary (Larionov, 1969). The effective porosity results (ϕe_D and ϕe_{ND}) were also compared for all lithological intervals, to evaluate the discrepancy (E) between these methods, expressed as:

$$E = |\overline{\phi e_{ND}} - \overline{\phi e_D}|, \qquad (6)$$

where ϕe_{ND} is the mean effective porosity value for a given lithological interval, obtained by the neutron-density method, while ϕe_D is the mean effective porosity value for a given lithological interval, obtained by the density method.

iv. The electrofacies models were created using the Multi-Resolution Graph-Based Clustering method. The log data input included: GR, RHOB, NPHI, ϕe_D, and ϕe_{ND}. The lithological intervals were inserted as "associated logs", functioning as a validation basis for the resulting models. In this manner, the software can relate the cluster samples (elements) to each one of the lithological intervals in the modeling process. The Euclidian metric was adopted in this work, as well as an initial number of 4 neurons in the Coarse-to-fine Self-Organizing Map (CFSOM). The MRGC method automatically provides an optimal number of clusters, though the user is allowed to manage the level of detail needed to characterize the electrofacies (Ye and Rabiller, 2000). It was set a minimum of 8 and a maximum of 12 initial clusters in the MRGC modeling process to attain a pattern of 8 final electrofacies for each model. In cases where the number of clusters was greater than 8, those with closer values of GR, RHOB and similar sample contingency were merged to satisfy the 8-electrofacies pattern. For each well, two types of models were created, each based on a different porosity log input in addition to the other geophysical logs (see Table 1).

RESULTS AND DISCUSSIONS

Database Structuring

The lithological intervals for each well (from AGP files) allowed us to determine and quantitatively analyze the total thicknesses of each unit in the wells, as can be seen in Figure 3a. Thus, it was possible to observe that the lithologies corresponding to diamictites represent the main intervals in both wells. The sandstone and siltstone intervals in both wells have very similar thicknesses; on the other hand, the intervals corresponding to shales are considerably different in both wells. Only in well 1GO-1-SC does a relatively thin interval of calcilutite (2 m) occur, and for this reason it was not considered in the calculations to determine the petrophysical parameters of this well.

Two lithostratigraphic profiles were prepared from the lithological data of each well (see Figure 3b). In these profiles, it was possible to observe two patterns of stratum succession: retrogradational and progradational. The lower portions of these two wells mainly comprise thinning upward cycles of the diamictites, followed by thickening upward cycles. This is an evident decrease and increase in energy and sediment input, respectively. On the other hand, only in the upper portion of the 1RCH-1-SC well profile does a retrogradational succession occur with a dominance

Table 1: Model identification, quantity of samples, number of initial clusters defined by the Geolog Software, and logs used to generate the electrofacies models. (LITH = lithology log; GR = gamma ray log; RHOB = bulk-density log; and Φ = porosity log).

Well	Model ID	Samples	Clusters	Logs			
				LITH	GR	RHOB	Φ
1GO-1-SC	GO1	3246	10	✓	✓	✓	NPHI
	GO2	3245	12	✓	✓	✓	ϕe_D
1RCH-1-SC	RC1	4758	9	✓	✓	✓	NPHI
	RC2	4758	10	✓	✓	✓	ϕe_{ND}

of sandstones at the base that are followed by shales (rhythmites?) at the top. This is a characteristic pattern of unconfined and confined (channeled) distal turbidite systems of the Taciba Formation. The basal portion of this succession is marked by a (probable) transgressive stratigraphic surface, which explains the increase in shale content in these strata.

Volume shale (V_{sh})

The results present differences according to the method used for the calculation of V_{sh}, as well as differences related to the lithological types of the wells. Table 2 exhibits minimum, maximum and mean values ($\overline{IGR}$ and $\overline{V_{sh_{Lar}}}$) of V_{sh} (V/V), obtained by the *IGR* and Larionov methods for each lithological intervals of the wells.

The Larionov method determined the absolute maximum V_{sh} value of 0.990 V/V for the shale interval, and the absolute minimum V_{sh} value of zero for the sandstone interval, for both wells. The mean V_{sh} values ($\overline{V_{sh_{Lar}}}$) are greater for the shale intervals and lower for the sandstone ones. In well 1GO-1-SC, V_{sh} mean values are greater than those in well 1RCH-1-SC for all intervals, except diamictite. In well 1GO-1-SC, diamictite and siltite intervals exhibit similar V_{sh} mean values.

The *IGR* method determined the absolute maximum V_{sh} value of 1 V/V for the shale interval and the absolute minimum V_{sh} value of zero for the sandstone interval, for both wells. The mean V_{sh} values ($\overline{IGR}$) are greater for the shale intervals and lower for the sandstone intervals. In well 1GO-1-SC, V_{sh} mean values using the *IGR* method are greater than those in well 1RCH-1-SC for all intervals, except diamictite.

Comparing the V_{sh} results (minimums, maximums and means) of each method, it is noticeable that the *IGR* method returns higher values than those determined by the Larionov's method. This effect is also noticed in the histograms of $V_{sh_{Lar}}$ and *IGR* for the complete lithological interval of the wells (see Figure 4). In wells 1GO-1-SC and 1RCH-1-SC, the discrepancy between the results (D) has its lowest values in the sandstone intervals, followed by shale, siltite and diamictite intervals. Conducting the equivalence comparison between intervals in the wells, it was possible to observe that the D values are similar. In general and considering that only the 1RCH-1-SC has the upper portion that is richer in shale (post-glacial distal turbidites), it is observed that the D values are very similar.

Effective Porosity (ϕe)

The effective porosity results present differences according to the method used for its determination, which are noticeable in terms of the lithological intervals of the wells. Table 3 exhibits minimum, maximum and mean values ($\overline{\phi e_D}$ and $\overline{\phi e_{ND}}$) of effective porosity (V/V), for each of the lithological intervals of the wells.

In the 1GO-1-SC well, the values of $\overline{\phi e_D}$ are similar or slightly lower than the values of $\overline{\phi e_{ND}}$ for each interval, so that the discrepancy of these means (E) is lower for the sandstone and siltite intervals (0.003 and 0.003, respectively), followed by diamictite and shale intervals (0.017 and 0.029, respectively). In this well, $\overline{\phi e_D}$ and $\overline{\phi e_{ND}}$ present similar values for the sandstone interval, 0.080 and 0.077, respectively (see Figure 5).

In well 1RCH-1-SC, the ϕe_D maximum values are remarkably higher than the ϕe_{ND} maximum values. This pattern extents for the mean porosity values ($\overline{\phi e_D}$ and $\overline{\phi e_{ND}}$) of each interval, so that the discrepancy of these means (E) is lower for the shale interval (0.027), followed by diamictite (0.049), siltite (0.053) and sandstone (0.085) intervals. In this well, the $\overline{\phi e_D}$ is 0.191 and the $\overline{\phi e_{ND}}$ is 0.106 for the sandstone intervals (see Figure 5).

According to França and Potter (1989), the porosity of the Itararé Group sandstones is of the intergranular type and secondary, representing approximately 10% of the rock volume. For 1GO-1-SC well, ϕe_D and ϕe_{ND} values for the sandstone interval corroborate the estimate given by these authors, while for 1RCH-1-SC well, only ϕe_{ND} values corroborate this estimate.

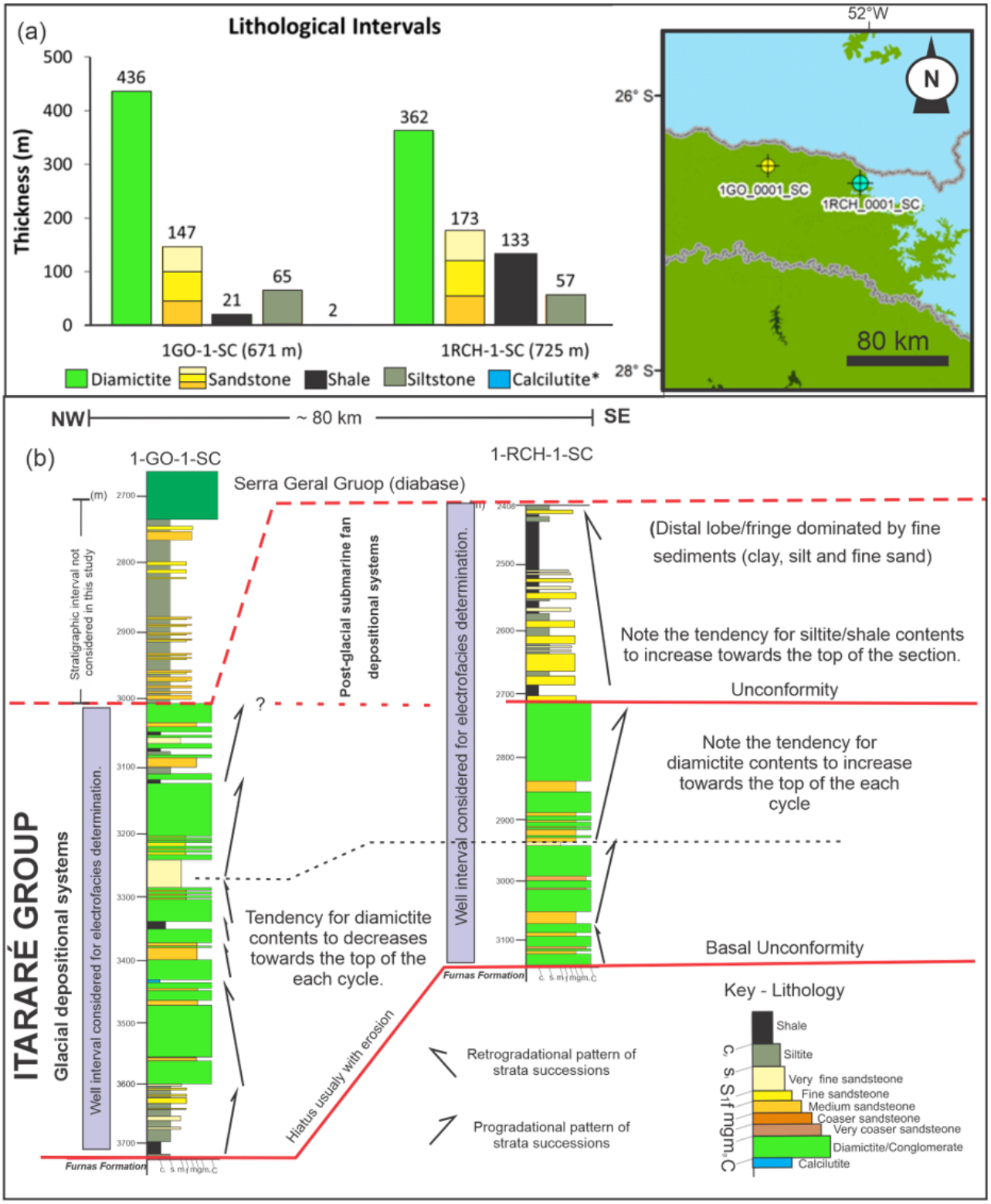

Figure 3: (a) Lithological intervals in wells 1GO-1-SC and 1RCH-1-SC: the lithological intervals represent the sum of all bed thicknesses of a given lithological unit. 671 m and 725 m are the sum of all interval thicknesses in each well. (b) Lithostratigraphic profiles from lithological data from each well.

Table 2: V_{sh} values (V/V) for wells 1GO-1-SC and 1RCH-1-SC. $\overline{V_{sh_{Lar}}}$ and $\overline{IGR}$ are the mean V_{sh} values for each lithological interval of the wells. The "Total" represents V_{sh} values for the complete studied stratigraphic intervals.

Well	**Interval**	$V_{sh_{Lar}}$			IGR			***D***
		min.	***max.***	$\overline{V_{sh_{Lar}}}$	***min.***	***max.***	$\overline{\boldsymbol{IGR}}$	
1GO-1-SC	Diamictite	0.074	0.706	0.338	0.146	0.825	0.500	0.162
	Sandstone	0	0.487	0.141	0	0.654	0.246	0.105
	Shale	0.306	0.990	0.631	0.474	1.000	0.760	0.129
	Siltstone	0.033	0.839	0.329	0.069	0.912	0.473	0.144
	Total	0	0.990	0.303	0	1.000	0.449	0.146
1RCH-1-SC	Diamictite	0.079	0.649	0.343	0.156	0.784	0.508	0.165
	Sandstone	0	0.479	0.133	0	0.646	0.236	0.103
	Shale	0.061	0.990	0.477	0.123	1.000	0.623	0.146
	Siltstone	0.092	0.650	0.291	0.178	0.785	0.448	0.157
	Total	0	0.990	0.314	0	1.000	0.459	0.145

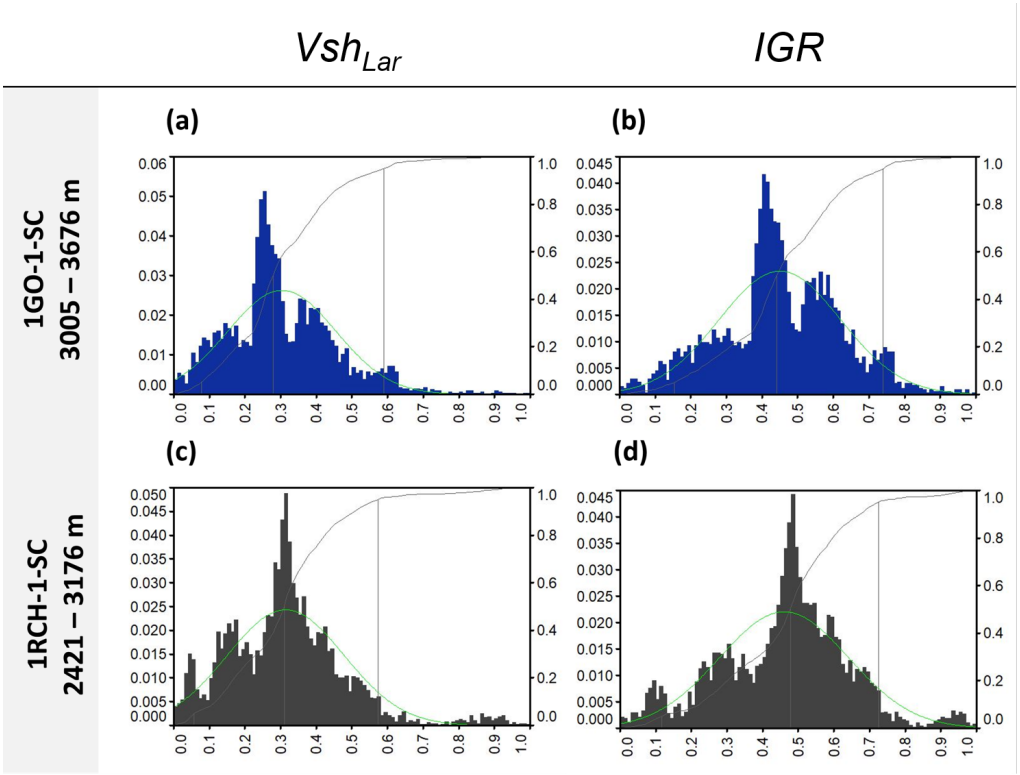

Figure 4: Comparative histograms of V_{sh} values determined by the Larionov method ($V_{sh_{Lar}}$) and gamma ray index (IGR) for wells 1GO-1-SC (a and b) and 1RCH-1-SC (c and d). Y axis (left side): frequency (fraction). Y axis (right side): accumulated fraction of data. X axis: volume shale (V/V). The depths are relative to the interval corresponding to the Itararé Group in the wells.

Table 3: Effective porosity (Φ_{eD} and Φ_{eND}) for wells 1GO-1-SC and 1RCH-1-SC. $\overline{\Phi_{eD}}$ and $\overline{\Phi_{e_{ND}}}$ represent the mean values for each lithological interval of the wells.

Well	**Interval**	$\boldsymbol{\Phi_{eD}}$			$\boldsymbol{\Phi_{eND}}$			***E***
		min.	***max.***	$\overline{\Phi_{eD}}$	***min.***	***max.***	$\overline{\Phi_{e_{ND}}}$	
1GO-1-SC	Diamictite	0	0.223	0.058	0.025	0.198	0.075	0.017
	Sandstone	0	0.258	0.080	0.018	0.229	0.077	0.003
	Shale	0	0.128	0.030	0	0.122	0.059	0.029
	Siltstone	0.007	0.230	0.075	0.020	0.214	0.078	0.003
	Total	0	0.258	0.063	0	0.229	0.075	0.012
1RCH-1-SC	Diamictite	0.069	0.199	0.118	0.016	0.122	0.069	0.049
	Sandstone	0	0.268	0.191	0.004	0.174	0.106	0.085
	Shale	0	0.239	0.111	0	0.198	0.084	0.027
	Siltstone	0.096	0.219	0.159	0.041	0.183	0.106	0.053
	Total	0	0.268	0.138	0	0.198	0.083	0.055

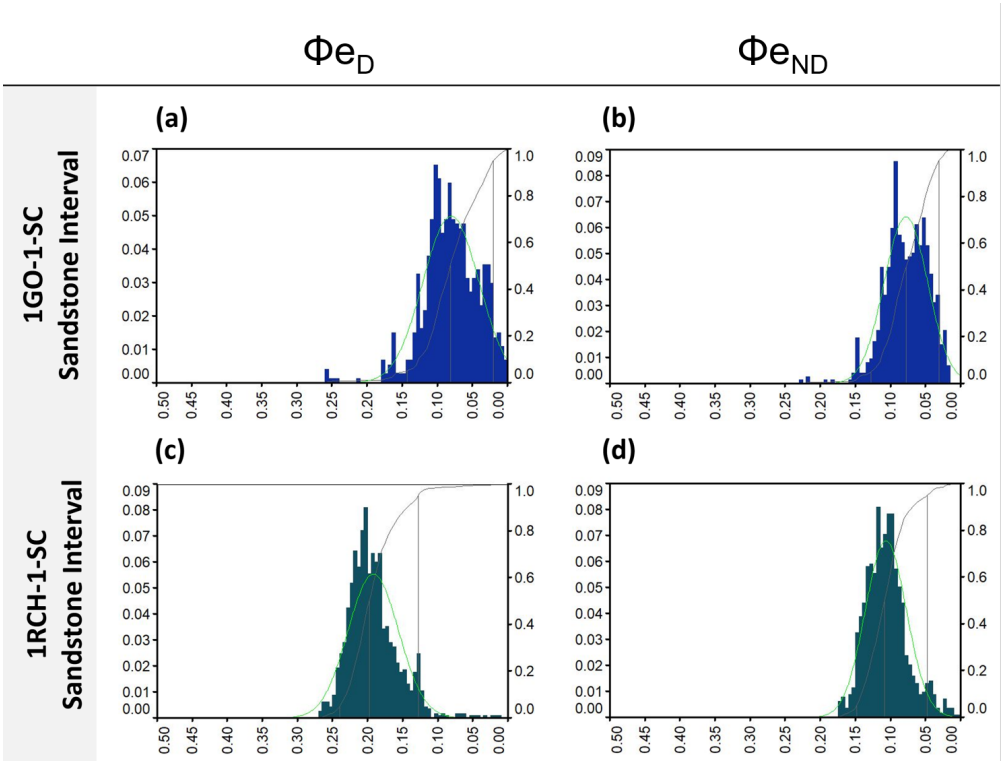

Figure 5: Comparative histograms of effective porosity values determined by the density method (ϕe_D) and neutron-density method (ϕe_{ND}) for the sandstone interval of wells 1GO-1-SC (a and b) and 1RCH-1-SC (c and d). Y axis (left side): frequency (fraction). Y axis (right side): accumulated fraction of data. X axis: effective porosity (V/V).

Electrofacies Models

Two electrofacies models were defined for each well: GO1 and GO2 (1GO-1-SC well); and RC1 and RC2 (1RCH-1-SC well). These models were represented in layout along with the lithological data and the geophysical curves used for the MRGC modeling process. The electrofacies were analyzed in relation to the lithologies of the wells, allowing the delimitation of the electrofacies associations (see Figures 6 and 7).

The sample contingency for all electrofacies models (after merging similar clusters) is shown in Table 4, where it is possible to verify the contribution of each lithological interval to the number of samples assigned to the electrofacies of the models, as well as its equivalent in percentage. The sample contingency was used as a reference to evaluate the representativeness of the electrofacies for the studied lithological intervals in the wells.

Table 5 groups representative data of the electrofacies determined for GO1, GO2, RC1 and RC2 models. The table exhibits mean values for GR, RHOB, and mean porosity values (NPHI, ϕe_D or ϕe_{ND}) for each electrofacies of the models. The weights refer to the total number of samples associated with each one of the electrofacies (see Tables 4 and 5). The visual representation of the electrofacies in the model layouts (see Figures 6 and 7) was given according to the colors displayed in Table 5.

Electrofacies of the GO1 and GO2 models

The A1 electrofacies presents the highest $\overline{GR}$ and $\overline{RHOB}$ values among the other electrofacies. The neutron porosity ($\overline{NPHI}$) for this electrofacies is higher than the effective porosity ($\overline{\phi e_D}$), which is probably associated to a higher shale content. The electrofacies is related to diamictites, shales and siltstones, comprising approximately 70%, 20% and 10% of the samples attributed to the electrofacies, respectively. This electrofacies is mainly recorded from 3020 to 3210 m and, subordinately, from 3340 to 3375 m. In these intervals, the A1 electrofacies is usually in association with the A2 and A3 electrofacies.

The A2 electrofacies has immediately lower $\overline{GR}$ values than those of the A1 electrofacies. However, the A2 electrofacies has the lowest $\overline{RHOB}$ values as well as the highest $\overline{NPHI}$ and $\overline{\phi e_D}$ values among the other electrofacies. The A2 electrofacies is related to diamictites, siltstones and shales, which comprise about 70%, 23% and 5% of the samples attributed to the electrofacies, respectively. The A2 electrofacies was mainly recorded at depths from 3050 to 3200 m. In this interval, the A2 electrofacies is in association with the A1 electrofacies. There are minor records of the A2 electrofacies below the depth of 3665 m, which are related to siltstones adjacent to sandstones. In general aspects, the A2 electrofacies is an electrofacies of anomalous characteristics in relation to bulk-density and porosity values. These characteristics may reflect the drilling conditions of the well, such as wall collapses, unconsolidated materials and instrumental errors during data collection, among others. The analysis of the caliper log may help in a better understanding of these conditions.

The A3 electrofacies has $\overline{GR}$ values close to 90 API, $\overline{RHOB}$ values of approximately 2640 kg/m3, and is related to diamictites and sandstones, comprising 90% and 6% of the samples attributed to the electrofacies, respectively. This electrofacies is recorded mainly at depths from 3005 to 3375 m, mostly where diamictites are next to shales or next to sandstones. In the first case, the A3 electrofacies is in association with the A1 electrofacies and, in the second, it is in association with the A4 electrofacies. In the GO1 model, there are also records of the A3 electrofacies below the depth of 3375 m, related to diamictites adjacent to sandstones. In this case, the A3 electrofacies is in association with the A4 electrofacies. The A3 electrofacies associations with other electrofacies suggest that there are areas of relatively gradual transition between diamictite and shale sections, and between diamictite and sandstone sections. The A3 electrofacies has the second highest weight of both models.

The A4 electrofacies present $\overline{GR}$ and $\overline{RHOB}$ values close to 75 API and 2605 kg/m3, respectively, and have the highest weight in GO1 and GO2 models. The mean porosity values ($\overline{NPHI}$ and $\overline{\phi e_D}$) are similar and relatively low ($\tilde{0}$.05 V/V). In the GO1 model, the A4 electrofacies is related to diamictite (78%), siltstones (12%) and sandstones (10%), and is mainly recorded at depths from 3305 to 3676 m, being primarily in association with A3 electrofacies and secondarily with A6, A8 or A5 electrofacies. In the GO2 model, the proportion of samples is approximately 84% (diamictites), 8% (siltstones) and 8% (sandstones), and the A4 electrofacies is recorded at depths from 3005 to 3360 m, usually in association with the A3 electrofacies in diamictite sections, and with the A6 and A7 electrofacies where diamictites intercalate with sandstones. At depths from 3400 to 3653 m, the A4 electrofacies is usually recorded in association with the electrofacies A5, A6 or A10, in diamictite or siltstone sections. In general aspects, the records of the A4 electrofacies are more homogeneous in both models, which is possibly a reflection of the electrofacies weight, being the highest among the other electrofacies.

The A5 electrofacies has the values 71 API for $\overline{GR}$ and 2420 kg/m3 for $\overline{RHOB}$, and is related to diamictites (63%), sandstones (25%) and siltites (12%). In the GO1 model, this electrofacies was recorded below the depth of 3247 m, where it is usually in association with the A4 electrofacies in diamictite sections, and with the A4 and A6 electrofacies in sandstone or siltstone sections. In the GO2 model, the A5 electrofacies was registered below 3055 m, exhibiting less records than observed in the GO1 model. In this case, this electrofacies is usually in association with the A4

Table 4: Contingencies (sample count): number of samples assigned to the electrofacies of the GO1, GO2, RC1 and RC2 models as a function of the lithological intervals of the Itararé Group. Percentual values are relative to the total number of samples in each electrofacies. The electrofacies total number of samples represents its weight in the model. *DM* = diamictite; *SS* = sandstone; *SH* = shale; *ST* = siltite.

Contingencies
(samples count)

ID	**Interval**	**A1**	**A2**	**A3**	**A4**	**A5**	**A6**	**A8**	**A9**
GO1	*DM*	335 (70%)	161 (71%)	659 (90%)	717 (78%)	172 (60%)	25 (14%)	15 (5%)	1 (1%)
	SS	4 (1%)	5 (2%)	45 (6%)	88 (10%)	85 (30%)	135 (77%)	238 (82%)	140 (99%)
	SH	84 (18%)	10 (4%)	8 (1%)	–	–	–	–	–
	ST	55 (12%)	52 (23%)	21 (3%)	110 (12%)	28 (10%)	15 (9%)	38 (13%)	–
	Total	478	228	733	915	285	175	291	141
ID	**Interval**	**A1**	**A2**	**A3**	**A4**	**A5**	**A6**	**A7**	**A10**
GO2	*DM*	244 (67%)	191 (68%)	450 (90%)	1000 (84%)	138 (67%)	55 (18%)	6 (2%)	1 (1%)
	SS	5 (1%)	3 (1%)	23 (5%)	103 (9%)	40 (19%)	198 (65%)	254 (95%)	110 (84%)
	SH	76 (21%)	20 (7%)	7 (1%)	2 (0%)	–	–	–	–
	ST	40 (11%)	65 (23%)	20 (4%)	87 (7%)	29 (14%)	50 (17%)	8 (3%)	20 (15%)
	Total	365	279	500	1192	207	303	268	131
ID	**Interval**	**B1**	**B2**	**B3**	**B4**	**B6**	**B7**	**B8**	**B9**
RC1	*DM*	–	65 (22%)	964 (65%)	388 (96%)	843 (73%)	93 (45%)	21 (2%)	–
	SS	–	1 (0%)	45 (3%)	–	84 (7%)	90 (44%)	716 (83%)	199 (99%)
	SH	144 (100%)	224 (75%)	269 (18%)	10 (2%)	189 (16%)	6 (3%)	29 (3%)	3 (1%)
	ST	–	7 (2%)	210 (14%)	5 (1%)	36 (3%)	16 (8%)	100 (12%)	1 (0%)
	Total	144	297	1488	403	1152	205	866	203
RC2	*DM*	–	52 (19%)	651 (69%)	578 (65%)	973 (76%)	21 (66%)	99 (11%)	–
	SS	–	–	18 (2%)	53 (6%)	81 (6%)	10 (31%)	691 (74%)	282 (99%)
	SH	123 (100%)	221 (80%)	189 (20%)	121 (14%)	190 (15%)	–	28 (3%)	2 (1%)
	ST	–	2 (1%)	84 (9%)	139 (16%)	38 (3%)	1 (3%)	111 (12%)	–
	Total	123	275	942	891	1282	32	929	284

Table 5: Identification, colors (hexadecimal code), weights and mean values of GR, RHOB and porosity (NPHI, Φ_{e_D} or $\Phi_{e_{ND}}$) of the electrofacies determined for the GO1, GO2, RC1 and RC2 models.

Model	ID	Color		Weight	$\overline{GR}$ (API)	$\overline{RHOB}$ (kg/m^3)	Porosity (V/V)
		Swatch	Hex Code				
1GO-1-SC							
							$\overline{NPHI}$
GO1	A1		#3533cc	478	110.23	2629.04	0.115
	A2		#a020f0	228	108.55	2232.23	0.190
	A3		#adff2f	733	88.55	2643.11	0.070
	A4		#da70d6	915	74.04	2603.14	0.056
	A5		#ffc0cb	285	71.99	2437.65	0.090
	A6		#d60005	175	58.35	2526.75	0.060
	A8		#ffaa00	291	42.60	2577.50	0.030
	A9		#ffd600	141	42.09	2473.28	0.070
							$\overline{\Phi_{e_D}}$
GO2	A1		#3533cc	365	112.00	2643.58	0.020
	A2		#a020f0	279	109.35	2275.82	0.139
	A3		#adff2f	500	93.86	2641.98	0.022
	A4		#da70d6	1192	76.82	2607.93	0.046
	A5		#ffc0cb	207	69.63	2406.77	0.160
	A6		#d60005	303	56.01	2568.01	0.060
	A7		#ff6300	268	50.88	2496.35	0.110
	A10		#ffff96	131	33.70	2610.27	0.040
1RCH-1-SC							
							$\overline{NPHI}$
RC1	B1		#006400	144	84.36	2665.48	0.210
	B2		#3533cc	297	67.69	2624.54	0.150
	B3		#a020f0	1488	57.40	2602.61	0.120
	B4		#adff2f	403	54.66	2655.11	0.082
	B6		#da70d6	1152	47.45	2633.85	0.050
	B7		#ff6300	205	37.77	2570.09	0.070
	B8		#ffd600	866	34.50	2501.43	0.110
	B9		#ffff96	203	20.44	2540.42	0.080
							$\overline{\Phi_{e_{ND}}}$
RC2	B1		#006400	123	85.80	2670.72	0.040
	B2		#3533cc	275	68.60	2616.86	0.110
	B3		#a020f0	942	61.00	2621.91	0.091
	B5		#9370db	891	53.28	2595.12	0.090
	B6		#da70d6	1282	48.00	2638.83	0.050
	B7		#ff6300	32	38.10	2566.28	0.080
	B8		#ffd600	929	35.58	2514.42	0.110
	B9		#ffff96	284	20.95	2527.41	0.100

electrofacies in diamictite sections, and with the A4 and A7 electrofacies in sandstone or siltstone sections. In general aspects, the A5 electrofacies presents few records within the models although its relationship to other electrofacies suggests that there are zones of a relatively gradual transition between diamictites and sandstones.

The A6 electrofacies has the values 57 API for $\overline{GR}$ and 2550 kg/m3 for $\overline{RHOB}$, and presents low porosity values. In the GO1 model, the A6 electrofacies is related to sandstones (77%), siltstones (19%) and diamictites (14%). In the GO1 model, the A6 electrofacies is recorded at depths from 3212 to 3475 m, in intervals of sandstones that are next to or intercalated with diamictites, and below the depth of 3630 m, in siltstone sections. In these intervals, the A6 electrofacies is in association with the A4, A5, A8 and A9 electrofacies. For the GO2 model, the proportion of samples is 65% (sandstone), 18% (diamictite) and 17% (siltstone). In the GO2 model, the A6 electrofacies was recorded at almost the same intervals mentioned for the GO1 model, although varying its distribution within the sections of occurrence and the electrofacies it associates with. In this case, the A6 electrofacies is usually in association with the A4 and A7 electrofacies at depths from 3212 and 3475 m, and with the A4 and A10 electrofacies below the depth of 3610 m.

The A7 electrofacies occurs only in the GO2 model, presenting the values 51 API for $\overline{GR}$ and 2496 kg/ m3 for $\overline{RHOB}$, and a $\overline{\phi e_D}$ value of 0.1 V/V. This electrofacies is almost entirely related to sandstones, comprising about 95% of the samples assigned to the electrofacies. In this model, the records of the A7 electrofacies are mainly related to sections of sandstones next to diamictites in the range from depths of 3217 to 3475 m, where it commonly associates the A6 and/or A4 electrofacies.

The A8 electrofacies, defined only in the GO1 model, presents the values 42 API for $\overline{GR}$ and 2575 kg/m3 for $\overline{RHOB}$, a low $\overline{NPHI}$ value (0.03 V/V), and is related to sandstones (83%), siltstones (12%) and diamictite (5%). In this model, this electrofacies is recorded below the depth of 3375 m, mainly in sandstone intervals that are next to diamictites or intercalated with siltstones. There are only minor records above this range. Additionally, this electrofacies is usually in association with the electrofacies A4, A6, A9 or A5 for the mentioned depth.

The A9 electrofacies (defined only in the GO1 model) presents a $\overline{GR}$ value like that of the previous electrofacies. Nevertheless, the $\overline{RHOB}$ value is lower and the $\overline{NPHI}$ one is higher than that of the A8 electrofacies. This electrofacies is related to sandstones, comprising 99% of the samples assigned to the electrofacies, being recorded mainly at depths from 3055 to 3475 m. In this interval, the A9 electrofacies is commonly seen in association with the A6 and A8 electrofacies.

The A10 electrofacies occurs only in the model GO2 and has a $\overline{GR}$ value of 34 API, being the lowest among the other electrofacies. This electrofacies presents the values of 2610 kg/m3 for $\overline{RHOB}$ and 0.04 V/V for $\overline{\phi e_D}$, and is related to sandstones (84%) and siltstones (15%) of the samples assigned to the facies. In this model, the A10 electrofacies is recorded at depths from 3560 to 3676 m, in sandstone intervals that are adjacent to siltstones, being commonly seen in association with the A6 and/or A4 electrofacies.

The GO1 and GO2 models comprise electrofacies in which the elements assigned to the diamictite interval predominate, followed by the sandstone interval. The shale interval represents only 3% of the total rock stacking of the Itararé Group in this well, reflecting in low numbers of samples and low representativeness within the models. Similarly, the siltstones exhibit low representativeness within the models, corresponding to less than 10% of the total rock stacking of the well.

Electrofacies of the RC1 and RC2 models

The B1 electrofacies presents the highest $\overline{GR}$ (85 API) and $\overline{RHOB}$ (2670 kg/m3) values among the other electrofacies. Neutron porosity means value ($\overline{NPHI}$) for the electrofacies is much higher than the effective porosity ($\overline{\phi e_{ND}}$), which is most likely related to the shale content of the samples, since the B1 electrofacies is exclusively related to shales (100% of the samples). In both models, the B1 electrofacies is mainly recorded from 2535 to 2942 m, presenting only a minor record above this range, which is in association with the B2 electrofacies.

The B2 electrofacies presents $\overline{GR}$ values close to 68 API and $\overline{RHOB}$ values slightly lower than that in the electrofacies B1. The $\overline{NPHI}$ value is higher than the $\overline{\phi e_{ND}}$ one, although the difference is less pronounced than that observed in the electrofacies B1. The B2 electrofacies is related to shales (78%) and diamictites (21%) and, in the RC1 model, is recorded in shale sections at depths from 2435 to 2700 m, and in diamictite sections at depths from 2700 to 2950 m. In these intervals, the B2 electrofacies is commonly seen in association with the electrofacies B3. In the RC2 model, the B2 electrofacies is recorded in shale sections at depths from 2435 to 2700 m and in diamictit sections at depths from 2700 to 2832 m. In these intervals, the B2 electrofacies is in association with the B3 and/or B5 electrofacies.

The B3 electrofacies has $\overline{GR}$ and $\overline{RHOB}$ values like those of the B2 electrofacies. The $\overline{NPHI}$ value is relatively close to the $\overline{\phi e_{ND}}$ one. This electrofacies is related to diamictites (68%), shales (21%) and siltstones (8%) of the samples assigned to the electrofacies. In the RC1 model, the B3 electrofacies was recorded at depths from 2421 to 2964 m, where one can identify: associations with B2 and B6 electrofa-

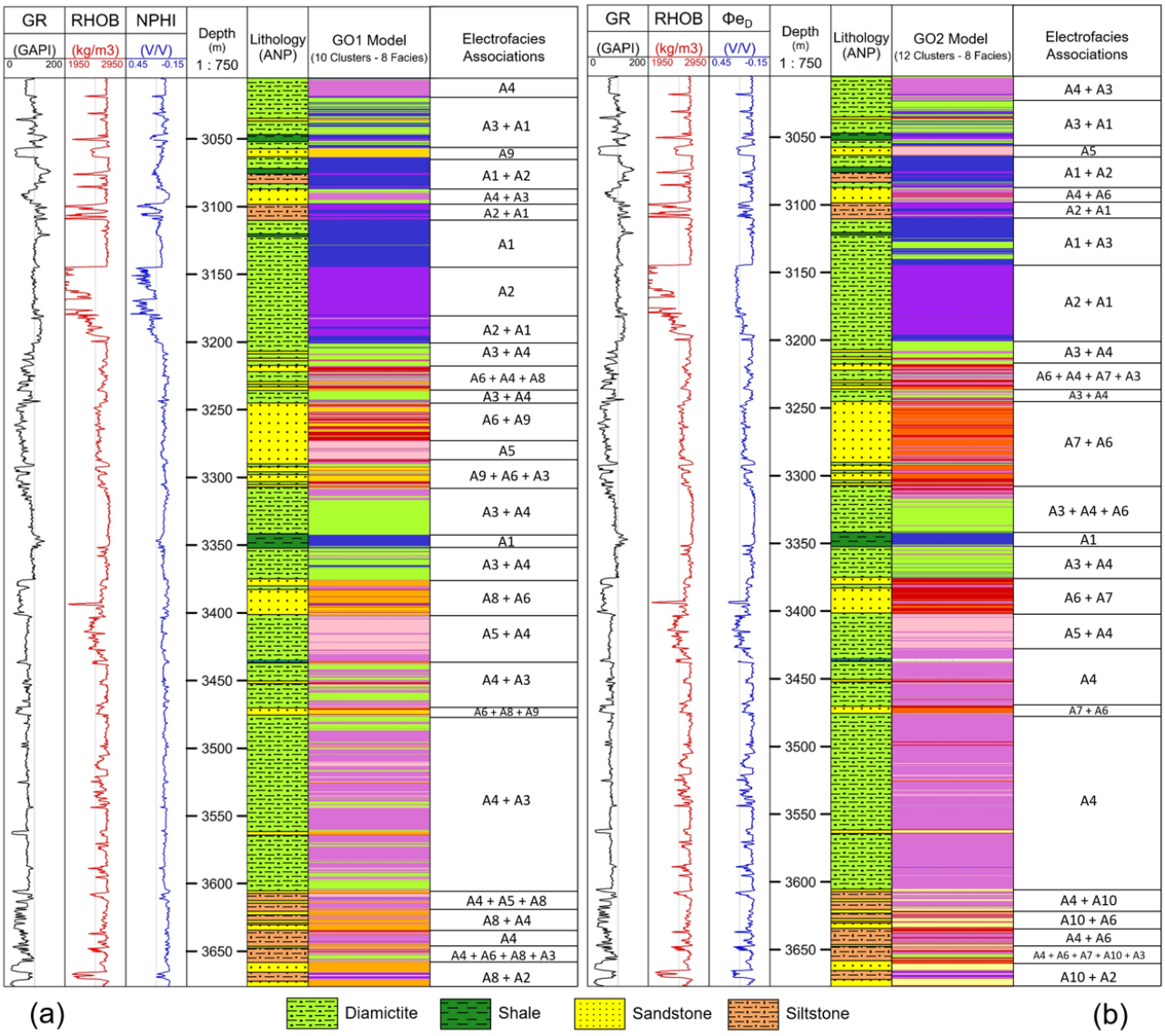

Figure 6: Models determined for the 1GO-1-SC well based on the neutron porosity log **(a)**, and effective porosity determined by the density method **(b)**.

cies in shale sections; associations with B2, B4 and B6 electrofacies in diamictite sections; and associations with B6 and B7 electrofacies in siltstone sections. In the RC2 model, the B3 electrofacies was recorded in shale sections at depths from 2421 to 2560 m, where it commonly associates with the B2 and B5 electrofacies and, in diamictite sections at depths from 2710 to 2970 m, where it frequently associates with the B2, B5 and B6 electrofacies. Ultimately, this electrofacies presents the highest weight in the RC1 model and the second highest one in the RC2 model.

The B4 electrofacies (defined only in the RC1 model) presents values 55 API for $\overline{GR}$ and 2655 kg/m3 for $\overline{RHOB}$, and a lower $\overline{NPHI}$ value lower than those of the previous electrofacies (0.08 V/V). This electrofacies is related to diamictites (96%) and shales (2%) of the samples attributed to the electrofacies. In this model, the B4 electrofacies is recorded at depths from 2770 to 2890 m, where it is associated with the B3 and B6 electrofacies, as well as at depths from 2960 to 3050 m, where it is associated only with the B6 electrofacies.

The B5 electrofacies, which occurs only in the RC2 model, presents $\overline{GR}$ and $\overline{RHOB}$ values slightly lower than those of the B4 electrofacies, an effective porosity ($\overline{\phi e_{ND}}$) of 0.09 V/V, and is related to diamictites (65%), siltstones (16%) and shales (14%). The B5 electrofacies is primarily recorded in diamictite sections at depths from 2710 to 2880 m and, secondarily, in shale and siltstone sections at depths from 2421 to 2670 m. In both intervals, the B5 electrofacies typically associates with the B3 and B6 electrofacies, with slight affiliations with the B2 electrofacies.

The B6 electrofacies presents 48 API for $\overline{GR}$, and 2635 kg/m3 for $\overline{RHOB}$, and $\overline{NPHI}$ and $\overline{\phi e_{ND}}$ coincident and low (0.05 V/V). This electrofacies is related to diamictites (75%), shales (15%) and sandstones (7%) of the samples attributed to the electrofacies. In the RC1 model, the B6 electrofacies is recorded at depths from 2475 to 2600 m, where it apparently delineates zones of transition (to sandstone sections) within shale or siltstone sections. Furthermore, this electrofacies is also related to diamictite sections at depths between 2883 and 3145 m, where they are commonly associated with the B4 electrofacies. In the RC2 model, the B6 electrofacies was registered in the same depth intervals described for the RC1 model. In the first one, the B6 electrofacies associates with the B5 electrofacies. In the second interval, it primarily associates with the B5 and B3 electrofacies and, secondarily, with the B8 electrofacies. Ultimately, this electrofacies presents the highest weight in the RC2 model and the second highest one in the RC1 model.

The B7 electrofacies exhibits the values 38 API for $\overline{GR}$ and 2570 kg/m3 for $\overline{RHOB}$, and mean porosity slightly higher than those of the B6 electrofacies, being $\overline{NPHI} < \overline{\phi e_{ND}}$. In the RC1 model, the B7 electrofacies is related to diamictites, sandstones and siltstones, comprising 45%, 44% and 8% of the samples assigned to the electrofacies, respectively, while this proportion is 66%, 31% and 3% for the same intervals of the RC2 model. The B7 electrofacies is mainly registered in intercalations of diamictites and sandstones at depths between 2890 and 2940 m, where they commonly associate with the B6 and/or B8 electrofacies.

The B8 electrofacies presents $\overline{GR}$ and $\overline{RHOB}$ values close to 35 API and 2510 kg/m3, respectively. In the RC1 model, the electrofacies B8 is related to sandstones, siltstones and diamictites, which comprise approximately 82%, 13% and 2% of the samples attributed to the electrofacies, respectively. In the RC2 model, the proportion is 74%, 12% and 11%, for these intervals. When compared to other electrofacies associated with sandstones, this electrofacies has the greatest mean porosity values, in which $\overline{NPHI} = \overline{\phi e_{ND}} = 0.11$ V/V. The B8 electrofacies is recorded across the Itararé Group interval in several well sections, in which it associates with the B3, B5 and B6 electrofacies, where sandstones and siltstones intercalate; with the B2, B3, B5 and B6 electrofacies, where sandstones and shales intercalate; and with the B6, B7 and B9 electrofacies, where sandstones are intercalated to diamictites or next to them.

The B9 electrofacies presents the lowest $\overline{GR}$ values ($\tilde{2}1$ API) and $\overline{RHOB}$ ones like those of the B8 electrofacies. The mean porosity values for the electrofacies B9 are slightly lower than those of the previous electrofacies, being $\overline{NPHI} < \overline{\phi e_{ND}}$. This factor is probably related to the shale content of the electrofacies, since it is almost entirely related to low GR sandstones (99% of the samples). In the RC1 model, the records are mainly below the depth of 2700 m, in sections of sandstone adjacent to diamictite, where the B9 electrofacies is commonly associated with the B7 and B8 electrofacies. In the RC2 model, the records extend to a broader range (depths of 2520 and 3074 m) of sandstone sections. In this case, electrofacies B9 commonly associates with electrofacies B8.

The RC1 and RC1 models also comprise electrofacies in which the elements assigned to the diamictite interval predominate, followed by the sandstone interval. Despite this condition, the RC1 and RC2 models received, proportionally, greater contributions of elements assigned to the shale and siltstone intervals than the models generated for well 1GO-1-SC.

CONCLUSIONS

In this study, a new workflow was used for electrofacies modeling, incorporating geophysical and geological information from two wells in the Itararé Group (Paraná Basin). The shale volume (V_{sh}) and effective porosity (ϕe) were determined and partially applied as petrophysical input parameters and helped to achieve an excellent correspondence between geological and petrophysical parameters. The main findings are presented as follows:

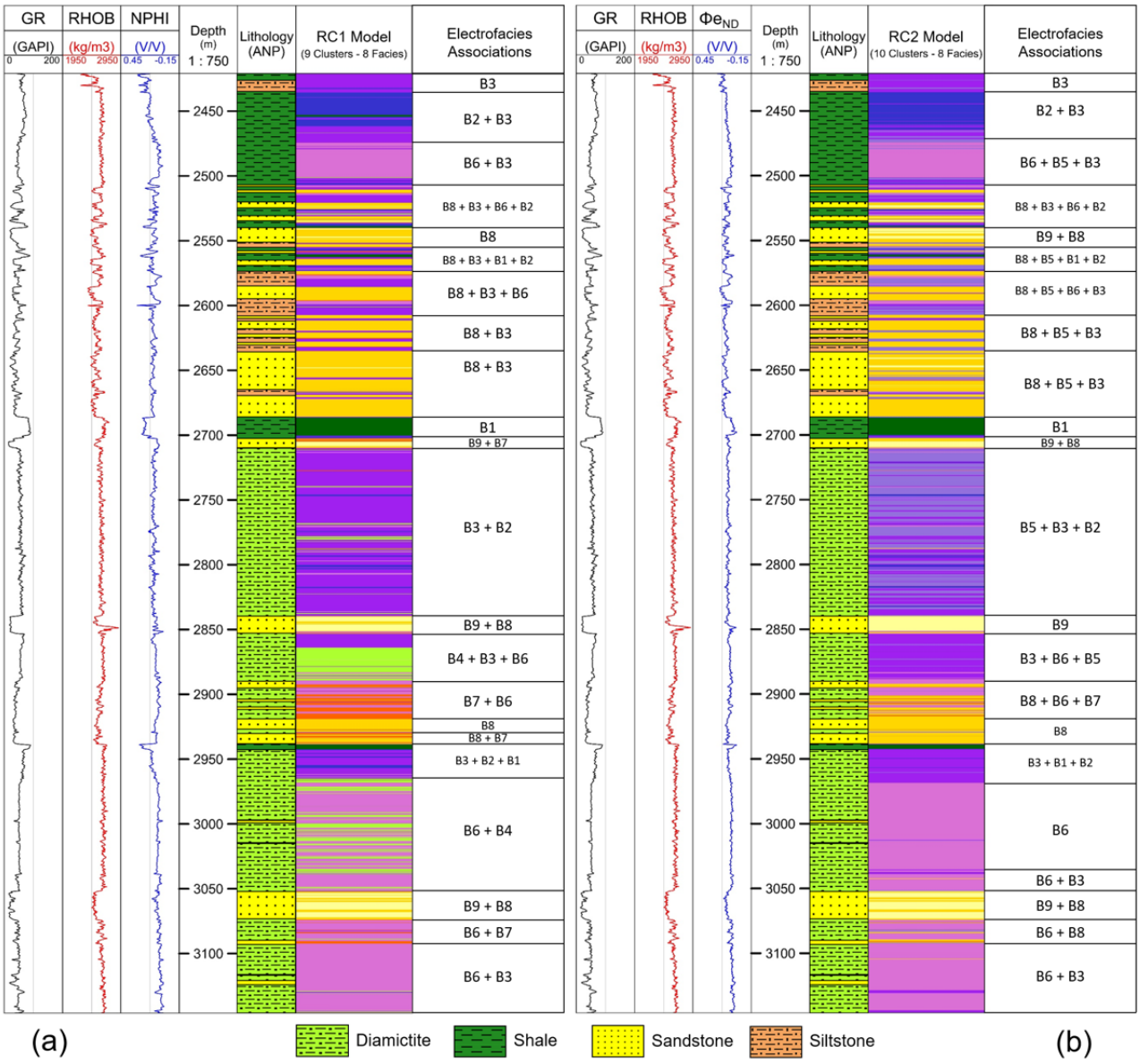

Figure 7: Models determined for well 1RCH-1-SC based on the neutron porosity log **(a)**, and effective porosity determined by the neutron-density method **(b)**.

i. The petrophysical parameters of volume shale (V_{sh}) and effective porosity (ϕe) were determined using different methodologies, which allowed a comparative evaluation for each of these parameters. The results exhibit differences that may be associated to the method of calculation of these parameters and/or the lithologies involved. The electrofacies models were elaborated with distinct input parameters for each well (GO1, GO2, RC1 and RC2), so that it allowed perceive heterogeneities within the lithologies of the wells, suggested the electrofacies were recorded along the well and according to the chosen parameters in the modeling process.

ii. The maximum, minimum and average values of Vsh from the linear method (IGR) are overestimated in comparison to the non-linear method (Larionov Equation), mainly for the sandstone and shale intervals, where V_{sh} is lower and higher, respectively. The ϕe_D method in well 1RCH-1-SC returned low-precision results when compared to the ϕe_{ND} method, specially to the sandstone interval (typical sandstone (ϕ_e) values available in the literature are about 0.1 V/V for the Itararé Group). The electrofacies models GO1 and GO2 suggest heterogeneities within the lithotypes of the analyzed wells: electrofacies A3, A4, A1, A2 and A5 for diamictites; and electrofacies A6, A7, A8, A9 and A10 for the sandstones. Shales are associated with the electrofacies A1 and A2, while siltstones are associated with electrofacies A1, A2 and A4. The RC1 and RC2 models also indicate heterogeneities throughout the wells: i) electrofacies B2 and B3 are associated with the top shales of well 1RCH-1-SC, while the others with the electrofacies B1; ii) electrofacies B3 and B5 (2,710 m), while the others are related to electrofacies B6 and B4; iii) the B8 electrofacies is more related to sandstones, while the electrofacies B7 occurs only in sandstones interbedded with diamictites and close to shales; iv) the electrofacies B9 (sandstones) occurs below 2,700 m. Models RC1 and RC2 relate the electrofacies B3, B5 or B6 to siltstones; however, they should not be considered representative only of this lithology, as they contribute only for 20% of the samples attributed to these electrofacies.

iii. In the GO1 and GO2 models, the MRGC modeling was efficient to determine diamictite and sandstone electrofacies. The GO1 model is relatively more accurate, considering diamictite and sandstone electrofacies, while the GO2 model was better for sandstones with low GR, associated to the electrofacies A10. These models are efficient in determining anomalous geophysical and petrophysical characteristics (electrofacies A2). In models RC1 and RC2, the electrofacies models were more efficient for diamictite, sandstone and shale. The RC1 and RC2 models present differences in the intervals with diamictite: i) the RC1 model recorded electrifications below 2,850 m, and ii) the RC2 model recorded more details in the diamictites.

iv. The sandstones of both wells presented mean porosity values (ϕe_D and ϕe_{ND}) that range from 0.077 to 0.101 V/V, which corroborate previous works of the Itararé Group, such as França and Potter (1989, 1991). Nonetheless, it is important to highlight that, specifically for the 1RCH-1-SC well, the ϕe_D value for sandstones is much higher than ϕe_{ND} (almost two times), which was one of the reasons for not using ϕe_D as an input log/parameter in the electrofacies-modeling of this well.

ACKNOWLEDGMENTS

This work was supported by the project *Técnicas Machine Learning para Reconhecimento de Padrões Sedimentológicos de Sistemas Turbidíticos - MLTurb* funded by PETROBRAS. The authors also thank to the Brazilian National Agency of Petroleum, Natural Gas and Biofuels (ANP) to provide the geophysical data, and to Emerson for training and the GEOLOG software license.

REFERENCES

Almeida, F. F. M., Y. Hasui, B. B. Brito Neves, and R. A. Fuck, 1977, Províncias Estruturais Brasileiras: VIII Simpósio de Geologia do Nordeste, Atas, Sociedade Brasileira de Geologia, 363–391.

Asquith, G., and C. R. Gibson, 1982, Basic Well Log Analysis for Geologists. Methods in Exploration, No. 3: AAPG.

Asquith, G., D. Krygowski, S. Henderson, and N. Hurley, 2004, Basic well log analysis. Methods in Exploration, No. 16: AAPG.

Bateman, R. M., and C. E. Konen, 1977, The Log Analyst and the Programmable Pocket Calculator: Part II – Crossplot Porosity and Water Saturation: The Log Analyst, **18**, 3–11.

Bocardi, L. B., L. A. Fernandes, S. D. Rostirolla, and C. J. Appi, 2006, Diagênese dos arenitos do Grupo Itararé, Permocarbonífero, Bacia do Paraná: Revista Brasileira de Geociéncias, **36**, 221–231, doi: 10.25249/0375-7536.2006362221231.

Buso, V. V., C. D. Aquino, P. S. G. Paim, A. L. Mori, C. Fallgatter, J. P. Milana, and B. Kneller, 2019, Late Palaeozoic Glacial Cycles and Subcycles in Western Gondwana: Correlation of Surface and Subsurface Data of the Paraná Basin, Brazil:

Palaeogeography, Palaeoclimatology, Palaeoecology, **531**, doi: 10.1016/j.palaeo.2017.09.004.

Eyles, C. H., N. Eyles, and A. B. França, 1993, Glaciation and tectonics in an active intracratonic Basin: the Late Palaeozoic Itararé Group, Paraná Basin, Brazil: Sedimentology, **40**, 1–25, doi: 10.1111/j.1365-3091.1993.tb01087.x.

França, A. B., 1987, Stratigraphy, depositional environment and reservoir analysis of the Itararé Group (Permo-carboniferous), Paraná Basin, Brazil: PhD thesis, University of Cincinnati, Cincinnati, Ohio, USA.

França, A. B., and P. E. Potter, 1988, Estratigrafia, ambiente deposicional e análise de reservatório do Grupo Itararé (Permocarbonífero), Bacia do Paraná (Parte 1): Boletim de Geociências da Petrobras, **2**, 147–191.

França, A. B., and P. E. Potter, 1989, Estratigrafia, ambiente deposicional do Grupo Itararé (Permocarbonífero), Bacia do Paraná (Parte 2): Boletim de Geociências da Petrobras, **3**, 17–28.

França, A. B., and P. E. Potter, 1991, Stratigraphy and reservoir potential of glacial deposits of the Itararé Group (Permo-carboniferous), Paraná Basin, Brazil: Bulletin of the American Association of Petroleum Geologists, **75**, 62–85.

Larionov, V. V., 1969, Borehole radiometry: Nedra, Moscow.

Malone, S. J., J. G. Meert, D. M. Banerjee, M. K. Pandit, E. Tamrat, G. D. Kamenov, V. R. Pradhan, and L. E. Sohl, 2008, Paleomagnetism and detrital zircon geochronology of the Upper Vindhyan sequence, Son Valley and Rajasthan, India: A ca. 1000 Ma closure age for the Purana Basins?: Precambrian Research, **164**, 137–159, doi: 10.1016/j.precamres.2008.04.004.

Meert, J. G., M. K. Pandit, V. R. Pradhan, J. Banks, R. Sirianni, M. Stroud, B. Newstead, and J. Gifford, 2010, Precambrian crustal evolution of peninsular india: A 3.0 billion year odyssey: Journal of Asian Earth Sciences, **39**, 483–515, doi: 10.1016/j.jseaes.2010.04.026.

Milani, E. J., 2004, Comentários sobre a origem e a evolução tectônica da Bacia do Paraná, *in* Geologia do Continente Sul-Americano: Evolução da obra de Fernando Flávio Marques de Almeida: Beca, Brazil, 239–265.

Milani, E. J., A. B. França, and R. L. Schneider, 1994, Bacia do Paraná: Boletim de Geociências da Petrobras, **8**, 69–82.

Milani, E. J., J. H. G. Melo, P. A. Souza, L. A. Fernandes, and A. B. França, 2007, Bacia do Paraná: Boletim de Geociências da Petrobras, **15**, 265–287.

Sagar, B. S. D., Q. Cheng, and F. Agterberg, 2018, Handbook of Mathematical Geosciences: Fifty Years of IAMG: Springer International Publishing.

Serra, O., and H. T. Abbott, 1982, The contribution of logging data to sedimentology and stratigraphy: Society of Petroleum Engineers Journal, **22**, 117–131, doi: 10.2118/9270-PA.

Ye, S. J., and P. Rabiller, 2000, A new tool for electrofacies analysis: Multi-resolution graph-based clustering: Presented at the SPWLA 41st Annual Logging Symposium. (4–7 June 2000).

Ye, S. J., and P. Rabiller, 2005, Automated electrofacies ordering: Petrophysics, **46**, 409–423.

Almeida, M. A.: conceptualization, database structuring, data request, evaluation and processing, petrophysical parameter calculation, electrofacies determination, result analysis, evaluation and interpretation, image preparation, writing – original draft preparation; **Nascimento, M. S.:** conceptualization, supervision (master's degree advisor), writing – original draft preparation; **Mota Alves, M. F.:** data evaluation and processing, density log (RHOB) data analysis, image preparation and interpretation.

Received on March 22, 2023 / Accepted on June 20, 2024